Functional characterization of a "plant-like" HYL1 homolog in the cnidarian *Nematostella vectensis* indicates a conserved involvement in microRNA biogenesis

Abhinandan Mani Tripathi[1], Arie Fridrich[1,2], Magda Lewandowska[1,2], Yehu Moran[1,3]

[1]Department of Ecology, Evolution and Behavior, Alexander Silberman Institute of Life Sciences, Faculty of Science, The Hebrew University of Jerusalem, Jerusalem 9190401, Israel

[2]These authors contributed equally to this work

[3]Corresponding author: yehu.moran@mail.huji.ac.il

Abstract

While the biogenesis of microRNAs (miRNAs) in both animals and plants depends on the RNase III Dicer, its helping partner proteins are considered distinct for each kingdom. Nevertheless, recent discovery of homologs of Hyponastic Leaves1 (HYL1), a "plant-specific" Dicer partner, in the metazoan phylum Cnidaria challenges the view that miRNAs evolved convergently in animals and plants. Here we show that the HYL1 homolog Hyl1-like a (Hyl1La) is crucial for development and miRNA biogenesis in the cnidarian model *Nematostella vectensis*: Inhibition of Hyl1La resulted in arresting of metamorphosis in *Nematostella* embryos and most of the miRNAs were significantly downregulated in Hyl1La knockdown animals. Further, immunoprecipitation followed by quantitative PCR revealed that in contrast to the plant HYL1, Hyl1La interacts only with precursor miRNAs and not with primary miRNAs. These results suggest that the last common ancestor of animals and plants carried a HYL1 homolog that took essential part in miRNA biogenesis.

Introduction

MicroRNAs (miRNAs) are 21-24 nucleotides-long small RNAs that are known to be involved in post-transcriptional gene regulation and play important roles in both plant and animal development (Alvarez-Garcia & Miska, 2005; Bråte et al., 2018; Voinnet, 2009). The miRNA is transcribed by RNA polymerase II into a long primary transcript, which is further processed into a miRNA precursor and finally chopped into ~22 nucleotide miRNA/miRNA* duplex (Bartel, 2004, 2018; Voinnet, 2009). The processing of miRNA varies between plants and animals (Moran et al., 2017). In animals, the biogenesis of miRNAs is compartmentalized as the processing occurs in both the nucleus and cytoplasm. Within the nucleus, the RNase type III Drosha and its partner Pasha (also called DGCR8) constitute a microprocessor complex (J. Han et al., 2004; Kim et al., 2009). This complex acts on primary miRNA (pri-miRNA) transcripts and process them into a precursor (pre-miRNA). The pre-miRNA is then transported by Exportin 5 into the cytoplasm where they get processed into the mature miRNA by the RNase type III Dicer with the help of other double-stranded RNA binding proteins such as Loquacious (Loqs), TRBP and PACT in the cytoplasm (J. Han et al., 2004; Redfern et al., 2013; Saito et al., 2005). Contrastingly, in plants both pri-miRNA and pre-miRNA are processed into mature miRNA by a single RNase type III, called DICER-LIKE1 (DCL1) assisted by its partner the double-stranded RNA binding motif (DSRM)-containing protein, Hyponastic Leaves1 (HYL1) within the nucleus (M.-H. Han et al., 2004; Voinnet, 2009). In both plants and animals, the miRNA duplex interacts with Argonaute proteins (AGOs) and forms the RNA-induced silencing complex (RISC) in the cytoplasm. The RISC complex commences miRNA guided cleavage or translational inhibition of complementary targets genes (Kim et al., 2009).

The metazoan lineages of Bilateria and its sister group Cnidaria separated more than 600 million years ago (MYA). While Bilateria include the vast majority of animals, Cnidaria include sea anemones, corals, hydroids and jellyfish. The phylogenetic position of cnidarians makes them an important comparative group for inferring animal evolution. In a previous study we identified different components of miRNA biogenesis machinery in Cnidaria and observed that most bilaterian components have cnidarian homologs. However, cnidarians lack homologs of classical bilaterian Dicer protein partners such as PACT, Loqs or TRBP (Moran et al., 2013). Interestingly two homologues of HYL1 called Hyl1-Like-a (NveHyl1La) and Hyl1-Like-b (NveHyl1Lb) were identified in the sea anemone *Nematostella vectensis* (Moran et al., 2013). Apart from this it was also found that cnidarian miRNAs possess several interesting features that are common to their counterparts in plants: cnidarian miRNAs and their targets show perfect complementarity and frequently regulate their targets by mRNA cleavage (Moran et al., 2014). Recently, some other common features with plants that were identified in *Nematostella* included methylation of miRNAs by HEN1 (Modepalli et al., 2018), a feature rarely found in animals and the origin of miRNAs from inverted duplication of their target genes (Fridrich et al., 2020), a feature previously considered specific to plant miRNAs.

In addition to the presence of HYL1 homologs in Cnidaria, homologs are also present in other non-bilaterian animals such as sponges (*Amphimedon queenslandica*) and in ctenophores (*Mnemiopsis leidyi*) (Fig. 1; Ref. (Moran et al., 2013). However, we could not detect HYL1 homologs in Placozoa (*T. adhaerens*) (Figure 1A). Additionally, we also could not find any homologs in bilaterian animals and in unicellular organism like Fungi and Ichthyosporea. However, deep phylogenetic study of DSRM proteins showed that those of protozoans and fungi are phylogenetically closer to the DSRM proteins of plants (Dias et al., 2017). These results suggested that the HYL1-like proteins were already present in the common ancestor of plants and animals and during evolution have been lost in Bilateria and Ichthyosporea. These sequence-based observations led us to experimentally test the function of a HYL1 homolog of *Nematostella,* which could provide better insight into the evolution and origin of the miRNA biogenesis pathway. Our results show that the knockdown of Hyl1La causes developmental arrest of *Nematostella* embryos and decreases miRNA levels. These results suggest that a HYL1 homolog is involved in *Nematostella* miRNA biogenesis indicating a common evolutionary history of miRNA biogenesis in plants and animals.

Results

Hyl1La plays an essential role in *Nematostella* development

Mutants of miRNA biogenesis pathway components exhibit severe developmental defects in both plants and animals (Alvarez-Garcia & Miska, 2005; Schauer et al., 2002). The HYL1 protein has been

known to play an essential role in growth and development of the model plant *Arabidopsis thaliana* by regulating miRNA biogenesis (Achkar et al., 2018; M.-H. Han et al., 2004). Similarly, in mice, TRBP mutants show multiple developmental abnormities and reduction in miRNA accumulation (Koscianska et al., 2011; Zhong et al., 1999). The *Hyl1La* gene of *Nematostella* contains 11 exons and 10 introns translating into a protein containing three DSRM domains (Figure 1B and Figure 2A). Unlike its paralog *Hyl1Lb* that is specific to stinging cells and carries unique protein domains, *Hyl1La* expression is ubiquitously distributed throughout *Nematostella* tissues and shares its domain structure with other cnidarian HYL1 homologs (Moran et al., 2013).Thus, we decided to focus our analysis on this gene. To decipher the function of Hyl1La in *Nematostella*, we designed two different splicing morpholinos (Hyl1La SI MO1 and Hyl1La SI MO2) to knockdown by mis-splicing the gene at two different intron-exons junctions. Additionally, the gene was also targeted for inhibition by using a translation-blocking morpholino (Hyl1La TB MO) which binds on the 5′ UTR and sterically blocks translation (Figure 2A). We injected each of the three MOs into *Nematostella* zygotes in parallel with a control morpholino (Control MO) designed to bind to no target in the sea anemone genome. The effect of SI MOs was validated by PCR followed by cloning and sequencing which revealed intron retention in both cases (Figure S1 and Table S1). All the injected animals were studied until nine days post-fertilization (dpf). We observed that more than 80% of the animals injected with control MO developed normally and metamorphosed into primary polyps. In contrast, the animals injected with any of the three Hyl1La MOs showed developmental abnormalities where more than 90% of the animals did not settle and metamorphosed into primary polyps until nine days post-fertilization (dpf) (Figure 2B-E). The developmental abnormalities observed here were grossly similar to those observed in *Nematostella* morphants of other miRNA processing components such as HEN1, Dicer1, AGO1 and AGO2 knockdown animals (Fridrich et al., 2020; Modepalli et al., 2018) . These results indicated that Hyl1La plays an essential role in *Nematostella* development, possibly by regulating the processing and expression of miRNAs.

Hyl1La regulates the miRNA biogenesis

The above observed developmental defects suggested the possible involvement of Hyl1La in miRNA biogenesis, as mutants defective in their miRNA biogenesis exhibit abnormal development in both animals and plants (Achkar et al., 2018; Zhong et al., 1999). The HYL1 in *Arabidopsis* interacts with the stem region of miRNA precursors by using their DSRM domains and work with DCL1 synergistically (Song et al., 2007). Although the Dicer alone is capable of processing the precursor into a mature miRNA, the presence of HYL1 is essential as it enhances the accuracy as well as efficiency of miRNA biogenesis in plants (Dong et al., 2008). To assay the possible role of Hyl1La on miRNA expression in *Nematostella*, we performed small RNA sequencing of animals, injected with Hyl1La SI MO1 and with control MO. The

analysis of read length distribution showed that the small RNA reads that lied between the size of miRNAs (20-24nt) were higher ($P < 0.01$) in control as compared to knockdown embryos (Figure 3A). Further, we analyzed the miRNA expression by using miRProf (Stocks et al., 2012) and normalized the miRNA reads in transcripts per million (TPM) (Table S2). For the miRNA quantification we used the most recent *Nematostella* miRNA datasets that were obtained by AGO-immunoprecipitation (Fridrich et al., 2020) . The expression of normalized miRNA reads was compared between control and Hyl1La SI MO1. About 54% of the total identified miRNAs showed downregulation of more than two-fold in Hyl1La SI MO1 injected animals as compared to the control (Figure 3B). Further, a significant reduction in overall miRNA abundance was observed in the knockdown morphants ($P < 0.00001$, Wilcoxon signed-rank test) (Figure 3C). The expression variation caused by the action of other two morpholinos (Hyl1La SI MO2 and Hyl1La TB) was also assayed by quantitative stem-loop PCR of five miRNAs (Figure 3D and Figure S2). A significant downregulation of three miRNAs: miR2022-3p, miR2025-3p and miR2026-5p was detected in all three MOs, which supported the small RNA sequencing results. In contrast, two miRNAs, miR2027-5p and miR2028-5p either showed upregulation or were not significantly affected by the Hyl1La knockdown. Previous studies have also shown that these two miRNAs may respond differently than other miRNAs in HEN1 and Dicer1 knockdown morphants of *Nematostella* (Modepalli et al., 2018). Further, we also checked for the processing accuracy of all the identified miRNAs by mapping them onto their respective precursors. The analysis did not reveal any aberrant processing. These results further suggested that like its homolog in plants, Hyl1La in *Nematostella* might be involved in enhancement of Dicer efficiency and is not involved in size selection.

To further support our results obtained with MOs, we attempted to knockdown this gene by using short-hairpin RNAs (shRNAs), a method previously established in *Nematostella* (Karabulut et al., 2019). We designed three different shRNAs from three different regions of Hyl1La gene (Hyl1La shRNA1, Hyl1La shRNA2 and Hyl1La shRNA3) (Figure 4A-C) and injected them into *Nematostella* zygotes. In parallel we also used a control shRNA with no target in *Nematostella* genome that was previously used as control for similar experiments (He et al., 2018; Karabulut et al., 2019). To assess the effect of these shRNAs on Hyl1La expression, we performed qRT-PCR from three days-old injected animals. Unexpectedly, we did not find any difference in Hyl1La expression (Figure 4D). Additionally, we also assessed the phenotype, but we could not identify any phenotypic difference as well. Next, we employed stem-loop PCR to test whether small RNAs are generated from an injected shRNA and indeed the small RNAs were produced as expected (Figure 4E). This result indicates that the small RNA derived from the shRNA were not able to down regulate Hyl1La.

Hyl1La interacts with pre-miRNAs but not with pri-miRNAs

The above observed reduction in miRNA expression indicates the possible involvement of Hyl1La in miRNA biogenesis. Being a DSRM containing protein, it can interact either with pri-miRNA or with pre-miRNA or with both. Hence to test if Hyl1La interacts with pre- and/or pri-miRNA we conducted an immunoprecipitation (IP) assay by injecting a plasmid carrying a cassette encoding an N-terminal 3×FLAG-tagged full-length Hyl1La ("FLAG- Hyl1La") followed by a 3′-mOrange2 separated by a P2A self-cleaving peptide (Figure 5A) (Kim et al., 2011; Shaner et al., 2008). The expression of the FLAG-Hyl1La cassette was confirmed by visualizing the animals under fluorescence microscope (Figure 5B) and by using anti-FLAG western blot (Figure S3A). Further, RNA immunoprecipitation (RIP) with anti-FLAG antibody was performed (Figure 5C) in three different biological replicates followed by PCR analysis. Interestingly, we observed that there was very poor enrichment of pri-miRNA (Ct-values >30, sometimes undetected) as compared to pre-miRNA (Table S4 and Figure S3 B-C). As expected, the poor enrichment of housekeeping gene (HKG4) (Columbus-Shenkar et al., 2018) was also observed in these RIP samples. Further, due to the very high Ct values measured for pri-miRNA we were not able to compare the levels of pri-miRNAs bound with IgG and accurately compare them to FLAG-Hyl1La. Interestingly, when we compared the enrichment of pre-miRNAs, we found that all of them were significantly enriched in FLAG-Hyl1La IP in comparison to IgG (Figure 5D and Figure S3C). These results showed that Hyl1La interacts with pre-miRNA but not with pri-miRNA.

Discussion

Altogether the absence of animal-like Dicer partner proteins such as TRBP or PACT and presence of a functional homolog of HYL1 (Hyl1La) in *Nematostella* indicated that a Hyl1-like protein might have been present in the last common ancestor of plants and animals. Apart from *Nematostella*, the presence of HYL1 homologs in additional members of Cnidaria and other non-bilaterian metazoan groups such as sponges (Figure 1A) further strengthens the notion of common ancestry of the miRNA systems of plants and animals. Further, unlike the cleavage mode of action and nearly-perfect target binding that could have evolved convergently in plants and cnidarians (Moran et al., 2014) due to functional constraints, the involvement in miRNA biogenesis of the Hyl1L in Cnidaria and its plant homolog HYL1 is far less likely to be the result of parallel evolution as it would require the independent recruitment of the same protein into the same system. Thus, our results call to reconsider the dominating hypothesis that microRNAs evolved convergently in plants and animals from an ancestral RNAi system (Axtell et al., 2011; Tarver et al., 2012). To the best of our knowledge, an evidence at the magnitude of our current finding of a miRNA-related HYL1-like activity supporting the alternative hypothesis that an elaborate miRNA pathway existed in the common ancestor of plants and animals was lacking until now. However, it is also important to note

that the presence of HYL1-like proteins by itself, cannot be considered a definitive hallmark for the existence of miRNAs in non-bilaterian animals or their relatives. For example, a homolog of HYL1 exists in the ctenophore *M. leidyi*, but this species does not produce miRNAs (Fig. 1; (Maxwell et al., 2012)). Moreover, several unicellular relatives of animals contain miRNAs, but no homologs of HYL1 (Bråte et al., 2018). Thus, this pathway might demonstrate in various lineages compositional flexibility as well as high loss rates (Reviewed in (Moran et al., 2017). Recently, it was found in *Chlamydomonas* (a unicellular green algae) that DUS16, which is a DSRM protein, and the RNase III DCL3 were efficient enough for miRNA processing (Yamasaki et al., 2016). Further, various fungal groups also exhibit the presence of Dicer and plant-like DSRM proteins and lack animal-like accessory proteins, such as Drosha and Pasha (Dang et al., 2011; Dias et al., 2017). Contrastingly, DCL3 of *Chlamydomonas* exhibits some structural features that are reminiscent of metazoan Drosha (Valli et al., 2016). These observations suggest that the common ancestor of all these groups might have harbored only a single Dicer/Drosha-like RNase III enzyme assisted by a DSRM protein resembling the ones found in plants (HYL1-like).

We unexpectedly found that in contrast to plant HYL1 proteins Hyl1La in *Nematostella* interacts only with pre-miRNA and not with pri-miRNA. A plausible explanation to this finding might be that *Nematostella* already possesses miRNA biogenesis machinery like the Drosha-Pasha microprocessor (Moran et al., 2013) that is known to interact only with pri-miRNAs and crop them into the pre-miRNAs (Kim et al., 2009). Another surprising finding in this study is that we were able to knockdown the Hyl1La by using the morpholino only and not by shRNA microinjection, despite the processing of the shRNA. A possible explanation for this contrasting result between MO and shRNA probably lies between the different mode of action of these two molecules. In contrast to MOs that do not use the cellular machinery, shRNA requires the miRNA/RNAi machinery for their production as well as in target recognition and inhibition. Thus, our combined results suggest that Hyl1La might have an additional effect on biogenesis steps that are downstream to the cleavage by Dicer such as loading of small RNAs into AGO, the protein at the heart of the RNA-induced silencing complex (RISC) (Hutvagner & Simard, 2008). Under such a condition the shRNA-derived small RNA would be unable to load onto RISC and hence could not cleave the Hyl1La, rendering its expression unaffected. Further, in such a scenario after injection with the shRNAs the system might reach a balance point that is very close to the normal Hyl1La levels. Alternatively, it is possible that the three shRNAs are ineffective due to lack of accessibility of the three distinct target sites on the Hyl1La transcript to the RISC loaded with the shRNA derived small RNAs for reasons such as secondary structure or binding by other proteins that restrict the RISC accessibility. However, we find this explanation less likely because the three shRNAs target distinct parts of this relatively long transcript.

Finally, here we report that Hyl1La plays an important role in miRNA biogenesis in *Nematostella*, a representative of Cnidaria which is the sister group of Bilateria. However, the functional importance of Hyl1La in *Nematostella* identified here raises another interesting evolutionary question of what led to the replacement of Hyl1La by other DSRM proteins like TRBP, Loqs or PACT in bilaterian animals during evolution (Figure 1A). Interestingly, both Loqs in flies and TRBP in mammals, enable processing of some miRNA precursors into different mature miRNAs and by this significantly increase their variability and targeted sequences (Fukunaga et al., 2012; Lee & Doudna, 2012). Such variability is currently unknown in plants or cnidarians. It is intriguing to consider the possibility that this ability of the bilaterian proteins to increase small RNA variability was advantageous over Hyl1-like proteins and led to the loss of the latter in bilaterian lineages.

MATERIALS AND METHODS

Animal culture and microinjection

Nematostella were in grown in 16‰ artificial sea water (ASW) at 18 °C in a dark culture room. The growing animals were fed with freshly hatched *Artemia salina* nauplii three times a week. Induction of spawning was performed as previously described (Genikhovich & Technau, 2009): the mature male and female animals were induced to produce eggs and sperm by placing them in an incubator for eight hours under constant white light and heat (25 °C). After induction, the tanks were further kept in 18 °C (in the culture room) for two hours to allow the release of egg packages and sperm. Further, the egg packages were fertilized for 30 min by placing the packages inside the male tanks. The quality of egg packages was checked under the stereomicroscope and egg packages of round shape and homogenous size were processed further for dejellying using 4% of L-Cysteine in 16‰ ASW pH 7.2 (titrated with 10 N NaOH). The selected eggs packages were kept in the cysteine solution for 45 min on a table shaker. The eggs were washed using 16‰ ASW in petri plates. These clean eggs (zygotes) were further used for microinjection. For micoinjection 1 mM stock solutions of both morpholino and shRNA were prepared by dissolving them into nuclease free water. The toxicity of morpholinos as well as shRNA was optimized by injecting different concentrations into the animals along with the control injected animals. Concentrations resulting in toxicity of less than 30% of the animals (estimated morphologically in the two days following the injection) were considered suitable for injection. All MOs used in this study were designed and synthesized by Gene Tools, LLC (USA).

Hyl1La TB MO (Translation Blocking) GGCCGCCATTTCTTAGAGAAGTTCA

Hyl1La SI MO1 (Splicing inhibition) AGAAACAGACTTGTACCTTTTTGTA

Hyl1La SI MO2 (Splicing inhibition) CTTGTTGTAGTCTAAGCCTTACCAT

Control MO (Standard control MO) CCTCTTACCTCAGTTACAATTTATA

We found that the optimum concentration was 300 µM, 900 µM and 450 µM for the Hyl1La TB, Hyl1La SI MO1 and Hyl1La SI MO2, respectively. For all the three shRNAs, 600 ng/µl concertation was found to be suitable. Similar concentration of control MO was used for micoinjection in parallel with Hyl1La MOs. In every shift we injected 600 zygotes (300 Control MO and 300 Hyl1La MO) by mixing the injected material with dextran Alexa Fluor 488 (Thermo Fisher Scientific, USA) which was used as a fluorescent tracer while injection was carried under magnification by a TS-100F fluorescent microscope (Nikon, Japan). The injected zygotes were kept at 22 °C for further growth. The morphology of the animals was observed up to nine days after which the number of settled and unsettled animals were counted and documented under SMZ-18 fluorescent stereomicroscope (Nikon). For RNA extraction micoinjected zygotes were flash frozen in liquid nitrogen after three days of growth and stored at -80 °C until RNA extraction. All the above experiments were performed in three independent biological replicates with three distinct animals' batches.

Small-RNA sequencing and analysis

The RNA was isolated using Trizol (Thermo Fisher Scientific) from three days old animals. Small RNA sequencing was performed for only Hyl1La SI MO1 and control MO injected animals. The small RNA library was prepared using NEBNext Multiplex Small RNA Library Prep Illumina kit (New England Biolabs, USA) with some modifications (Plotnikova et al., 2019). In brief, small RNAs were isolated (18nt-30nt) from 1 µg of total RNA using 15% urea-PAGE (Bio-Rad, USA) followed by overnight precipitation using 0.3% NaCl. The size-selected small RNAs were further precipitated using ice-cold ethanol (2.5× volume) and 1 µl of GlycoBlue (Thermo Fisher Scientific) by centrifugation at 21130 × *g*. The pellet was dissolved in 7.5 µl nuclease free water and used further for adapter ligation. The ligated products were subjected to 14 cycles of PCR amplification using adapter specific primers. The PCR product was run on 2% agarose gel followed by staining with GelRed (Biotium, USA). The band size between 137nt–149nt was selected and purified using Gel Extraction Kit (Macherey-Nagel, Germany). The quality of purified product (sRNA-seq libraries) was checked by using TapeStation system (Agilent, USA). The libraries having a dominant peak at the the size range of 137nt–149nt were used for sequencing. One ng of each sample was run on NextSeq500 (Illumina) in single end mode.

The small RNA data was analysed using miRProf (Stocks et al., 2012) with the following parameters: two mismatches allowed, minimum abundance 1, allowed overhang and not grouping mature

and star strands. For mapping onto the genome and miRNA precursor for identification of aberrant processing of small RNAs miRDeep2 (Friedländer et al., 2012) was used. The miRNA expression was normalized in TPM (transcripts per million) by using only the transcripts that mapped on the reference genome. For read length distribution and scattered plot we used the average of expression obtained from the three biological replicates.

Synthesis of shRNA

Potential shRNA precursors for Hyl1La gene were predicted using the shRNA prediction tools (https://www.invivogen.com/sirnawizard/index.php) (Karabulut et al., 2019). Three precursors from three different regions were further chosen, all having GC content of more than 35%. Further, we also added to the sequence a T7 promotor and three different mismatches at nucleotide positions 10, 13 and 16 to create bulges in the precursors (Figure 4 A-C). All these modified precursors were reverse complemented and synthesized at the DNA level by Integrated DNA Technologies (USA). The DNA templates and reverse primer were mixed (1:1) and denatured at 98 °C for 5 min and cooled to 24 °C. Further, this mixture was mixed with the components of in-vitro transcription kit (Epicentre, USA) and incubated for eight hours at room temperature. The in-vitro transcribed product was further purified using a cleaning kit (Zymo Research, USA). The quality and size of the precursor was checked on agarose gel and its concentration was measured using Qubit RNA BR (Broad Range) Assay Kit with the Qubit Fluorometer (Thermo, USA). The concentration ranged from 1500 ng/µl to 2000 ng/µl.

Reverse transcription-quantitative PCR

For the quantification of Hyl1La transcripts from shRNA injected animals and for checking the splicing inhibition (Hyl1La SI MO injected animals), cDNA was prepared from 500 ng of total RNA using the iScript™ cDNA Synthesis Kit (Bio-Rad). For the quantification of miRNAs and shRNA, we designed the stem loop primers for five different miRNAs and shRNA (Chen et al., 2005). For cDNA preparation, 100 ng of total RNA was reverse transcribed using the SuperScript™ III Reverse Transcriptase (Thermo Fisher Scientific). The specificity of the miRNA primers was determined by using end point PCR (Varkonyi-Gasic et al., 2007). For this, we used 2 µl of cDNA as template, miRNAs specific forward primer and stem-loop specific reverse primer and run the PCR at 94 °C for 2 min, followed by 35 cycles of 94 °C for 15 s and 60 °C for 1 min. For analyzing differential expression, we ran qRT-PCR with 5sRNA as internal control. For all the real time experiments, we used Fast SYBR® Green Master Mix (Thermo Fisher Scientific) and samples were run on StepOnePlus Real-Time PCR System (Thermo Fisher Scientific). All the real time experiments were performed in three independent biological and two technical replicates and

data was analysed using $2^{-\Delta\Delta Ct}$ method (Livak & Schmittgen, 2001). All the primers are listed in Table S3.

Cloning and sequencing of Hyl1La SI MO injected animals

To validate the effect of splicing morpholinos, we designed the primers pairs spanning the introns lying on the boundary of exons. PCR of the Hyl1La was done using Q5® High-Fidelity DNA Polymerase (New England Biolabs). The PCR products were run on the gel and the expected-sized PCR product was purified with a kit. Then the purified PCR products were ligated into the pJet2.1 vector (Thermo Fisher Scientific) and transformed into the *E. coli* DH5α strain. The plasmids were purified by a PureLink miniprep kit (Thermo Fisher Scientific) and outsourced for Sanger sequencing (HyLabs, Israel).

Plasmid generation

Two gBlock synthetic DNA fragments (Integrated DNA Technologies, USA) at the lengths of 1.6 kb and 1.7 kb corresponding to Hyl1La fragments with a 3×FLAG tag and 20 bp overlaps were ordered used for generating the expression cassette. These fragments were PCR-amplified by Q5® Hot Start High-Fidelity DNA Polymerase (New England Biolabs), visualized on 1% agarose gel and purified by NucleoSpin Gel and PCR Clean-up (Macherey-Nagel). Gibson assembly was performed with the NEBuilder HiFi DNA Assembly Master Mix (New England Biolabs) following manufacturer's protocol. The resulting product was further subcloned by restriction digestion with *Asc*I and *Sal*I into a pER242 vector having a TBP promoter previously proved to drive ubiquitous expression in *Nematostella* (Admoni et al., 2020), mOrange2, and SV40 polyadenylation signal (Figure 5A). The transformation was performed in *E. coli* DH5α strain (New England Biolabs). The plasmid was purified by PureLink™ HiPure Plasmid Midiprep Kit (Thermo Fisher Scientific) and sequenced by the Sanger method (HyLabs, Israel). 100 ng of purified plasmid was injected into the fertilized *Nematostella* embryo and visualized after two days under an SMZ18 stereomicroscope equipped with a DS-Qi2 camera (Nikon, Japan).

Hyl1La immunoprecipitation

100 µl of protein G SureBeads™ magnetic beads (Bio-Rad, USA) were washed five times with 1× PBS (Phosphate-buffered saline). 5 µg of monoclonal mouse anti-FLAG M2 antibody (Sigma-Aldrich, USA) or total mouse IgG (Sigma-Aldrich) were added to the washed beads and incubated overnight at 4 °C on a rotating shaker. Three thousand zygotes were injected with the plasmid containing 3×FLAG-Hyl1La among which ~ 2000 animals survived after two days and were used for protein extraction. Protein was extracted in lysis buffer with following composition: 25 mM Tris-HCl (pH 7.4), 150 mM KCl, 25 mM EDTA, 0.5% NP-40, 1 mM DTT, Protease inhibitor cOmplete ULTRA tablets (Roche, Germany) and

Protease Inhibitor Cocktail Set III, EDTA-Free (Merck Millipore, USA). Murine RNase inhibitor (New England Biolabs) was used in RNA processing buffer. The RNase and protease inhibitor were added fresh just before use. For protein extraction, the frozen animals were mechanically homogenized in 1 ml lysis buffer and incubated for rotation at 4 °C. After two hours the samples were centrifuged at 16000 × *g* for 15 min at 4 ºC and supernatant was collected and stored in -80 ºC. The next day, 100 µl of protein G magnetic beads were washed thrice with 1 ml 1×PBS, once with lysis buffer and then mixed with the protein lysate. The tube volume was maintained to 1.2 ml using the lysis buffer containing RNase inhibitor and incubated at 4 °C on a rotating shaker for one hour. After one hour, the pre-cleared lysate was collected and added to the antibody-bound beads that were preincubated with the antibody overnight. These samples were incubated for 2 h in rotation at 4 ºC. After incubation the beads were collected by using a magnetic stand and washed with lysis buffer containing RNase inhibitor six times and one time with PBS with RNAse inhibitor. For western blot 40 µl SDS sample buffer (New England Biolabs) were added to the beads and heated at 100 °C for 8 min and placed on ice for 1 min. The samples were then centrifuged for 1 min at 16,000 × *g* at 4 °C, and the supernatant was collected.

For RNA extraction, the beads were mixed with 1 ml Trizol (Thermo Fisher Scientific) and purified following the manufacturer's protocol. To increase the yield, we added 1 µl of RNA-grade glycogen (Thermo Fisher Scientific) into the isopropanol during the precipitation step. The isolated RNA was treated with Turbo DNAse (Thermo Fisher Scientific) for 30 min at 37 °C, purified with RNA Clean & Concentrator-5 kit (Zymo Research), eluted in 8 µl and used for cDNA preparation.

Primer designing for pre- and pri-miRNA quantification

The pre- and pri-miRNA transcripts of five different miRNAs were quantified. The pre-miRNA primer pairs were designed from stable stem region of precursors (Figure S4) as described previously (Schmittgen et al., 2008). The pre-miRNA sequence was obtained from our recently published data (Fridrich et al., 2020). The primer pairs for pri-miRNA were designed so they will anneal at least 10 nucleotides away from the pre-miRNA primers (Figure S5). These probable pri-miRNA sequences flanking the pre-miRNA were obtained from the *Nematostella* genome browser (https://simrbase.stowers.org/).

Quantification and statistical analysis

For statistical analysis of qRT-PCR data, Student's t-test (paired two-tailed) was performed on ΔCt values between different comparisons. For phenotypic analysis we performed Student's t-test between the number of developed and undeveloped animals. To check overall significant difference between the miRNA expression levels, Wilcoxon signed-rank test was done. The Student's t-test was conducted in

Microsoft Excel while Wilcoxon signed-rank test was done using socscistatistics (https://www.socscistatistics.com/tests/signedranks/default.aspx).

Acknowledgments

The authors would like to thank Dr. Michal Bronstein and Ms. Adi Turjeman of the Centre for Genomic Technologies (The Hebrew University) for their help with sequencing. The authors would also like to thank Dr. Reuven Aharoni (The Hebrew University) for his technical and administrative assistance in this work. This work was supported by European Research Council Starting Grant 637456 CNIDARIAMICRORNA and European Research Council Consolidator Grant 863809 AntiViralEvo to YM.

Author contributions

Conceptualization: A.M.T. and Y.M.; Methodology: A.M.T. and Y.M.; Validation: A.M.T.; Software: A.M.T. and A.F.; Formal Analysis: A.M.T., A.F. and M.L.; Investigation: A.M.T., A.F. and M.L.; Resources: Y.M.; Data Curation: A.M.T.; Writing –Original Draft: A.M.T. and Y.M.; Writing –Review & Editing: A.F. and M.L.; Visualization: A.M.T. and A.F.; Supervision: Y.M.; Project Administration: Y.M.; Funding Acquisition: Y.M.

Additional files

Supplementary files

Supplementary files include fivefigures and four tables (Table S1, Table S2, Table S3 and Table S4).

Data availability

The small RNA sequencing data were submitted to NCBI-SRA under BioProject ID PRJNA630340.

References

Achkar, N. P., Cho, S. K., Poulsen, C., Arce, A. L., Re, D. A., Giudicatti, A. J., Karayekov, E., Ryu, M. Y., Choi, S. W., & Harholt, J. (2018). A quick HYL1-dependent reactivation of microRNA production is required for a proper developmental response after extended periods of light deprivation. *Developmental cell*, *46*(2), 236-247. e236.

Admoni, Y., Kozlovski, I., Lewandowska, M., & Moran, Y. (2020). TATA Binding Protein (TBP) Promoter Drives Ubiquitous Expression of Marker Transgene in the Adult Sea Anemone Nematostella vectensis. *Genes*, *11*(9), 1081.

Alvarez-Garcia, I., & Miska, E. A. (2005). MicroRNA functions in animal development and human disease. *Development*, *132*(21), 4653-4662.

Axtell, M. J., Westholm, J. O., & Lai, E. C. (2011). Vive la différence: biogenesis and evolution of microRNAs in plants and animals. *Genome biology*, *12*(4), 1-13.

Bartel, D. P. (2004). MicroRNAs: genomics, biogenesis, mechanism, and function. *Cell*, *116*(2), 281-297.

Bartel, D. P. (2018). Metazoan micrornas. *Cell*, *173*(1), 20-51.

Bråte, J., Neumann, R. S., Fromm, B., Haraldsen, A. A., Tarver, J. E., Suga, H., Donoghue, P. C., Peterson, K. J., Ruiz-Trillo, I., & Grini, P. E. (2018). Unicellular origin of the animal microRNA machinery. *Current Biology*, *28*(20), 3288-3295. e3285.

Chen, C., Ridzon, D. A., Broomer, A. J., Zhou, Z., Lee, D. H., Nguyen, J. T., Barbisin, M., Xu, N. L., Mahuvakar, V. R., & Andersen, M. R. (2005). Real-time quantification of microRNAs by stem–loop RT–PCR. *Nucleic acids research*, *33*(20), e179-e179.

Columbus-Shenkar, Y. Y., Sachkova, M. Y., Macrander, J., Fridrich, A., Modepalli, V., Reitzel, A. M., Sunagar, K., & Moran, Y. (2018). Dynamics of venom composition across a complex life cycle. *Elife*, *7*, e35014.

Dang, Y., Yang, Q., Xue, Z., & Liu, Y. (2011). RNA interference in fungi: pathways, functions, and applications. *Eukaryotic cell*, *10*(9), 1148-1155.

Dias, R., Manny, A., Kolaczkowski, O., & Kolaczkowski, B. (2017). Convergence of domain architecture, structure, and ligand affinity in animal and plant RNA-binding proteins. *Molecular biology and evolution*, *34*(6), 1429-1444.

Dong, Z., Han, M.-H., & Fedoroff, N. (2008). The RNA-binding proteins HYL1 and SE promote accurate in vitro processing of pri-miRNA by DCL1. *Proceedings of the National Academy of Sciences*, *105*(29), 9970-9975.

Fridrich, A., Modepalli, V., Lewandowska, M., Aharoni, R., & Moran, Y. (2020). Unravelling the developmental and functional significance of an ancient Argonaute duplication. *Nature communications*, *11*(1), 1-12.

Friedländer, M. R., Mackowiak, S. D., Li, N., Chen, W., & Rajewsky, N. (2012). miRDeep2 accurately identifies known and hundreds of novel microRNA genes in seven animal clades. *Nucleic acids research*, *40*(1), 37-52.

Fukunaga, R., Han, B. W., Hung, J.-H., Xu, J., Weng, Z., & Zamore, P. D. (2012). Dicer partner proteins tune the length of mature miRNAs in flies and mammals. *Cell*, *151*(3), 533-546.

Genikhovich, G., & Technau, U. (2009). Induction of spawning in the starlet sea anemone Nematostella vectensis, in vitro fertilization of gametes, and dejellying of zygotes. *Cold Spring Harbor Protocols*, *2009*(9), pdb. prot5281.

Han, J., Lee, Y., Yeom, K.-H., Kim, Y.-K., Jin, H., & Kim, V. N. (2004). The Drosha-DGCR8 complex in primary microRNA processing. *Genes & development*, *18*(24), 3016-3027.

Han, M.-H., Goud, S., Song, L., & Fedoroff, N. (2004). The Arabidopsis double-stranded RNA-binding protein HYL1 plays a role in microRNA-mediated gene regulation. *Proceedings of the National Academy of Sciences*, *101*(4), 1093-1098.

He, S., Del Viso, F., Chen, C.-Y., Ikmi, A., Kroesen, A. E., & Gibson, M. C. (2018). An axial Hox code controls tissue segmentation and body patterning in Nematostella vectensis. *Science*, *361*(6409), 1377-1380.

Hutvagner, G., & Simard, M. J. (2008). Argonaute proteins: key players in RNA silencing. *Nature reviews Molecular cell biology*, *9*(1), 22-32.

Karabulut, A., He, S., Chen, C.-Y., McKinney, S. A., & Gibson, M. C. (2019). Electroporation of short hairpin RNAs for rapid and efficient gene knockdown in the starlet sea anemone, Nematostella vectensis. *Developmental biology*, *448*(1), 7-15.

Kim, J. H., Lee, S.-R., Li, L.-H., Park, H.-J., Park, J.-H., Lee, K. Y., Kim, M.-K., Shin, B. A., & Choi, S.-Y. (2011). High cleavage efficiency of a 2A peptide derived from porcine teschovirus-1 in human cell lines, zebrafish and mice. *PloS one*, *6*(4), e18556.

Kim, V. N., Han, J., & Siomi, M. C. (2009). Biogenesis of small RNAs in animals. *Nature reviews Molecular cell biology*, *10*(2), 126-139.

Koscianska, E., Starega-Roslan, J., & Krzyzosiak, W. J. (2011). The role of Dicer protein partners in the processing of microRNA precursors. *PloS one*, *6*(12).

Lee, H. Y., & Doudna, J. A. (2012). TRBP alters human precursor microRNA processing in vitro. *Rna*, *18*(11).

Livak, K. J., & Schmittgen, T. D. (2001). Analysis of relative gene expression data using real-time quantitative PCR and the 2− ΔΔCT method. *methods*, *25*(4), 402-408.

Maxwell, E. K., Ryan, J. F., Schnitzler, C. E., Browne, W. E., & Baxevanis, A. D. (2012). MicroRNAs and essential components of the microRNA processing machinery are not encoded in the genome of the ctenophore Mnemiopsis leidyi. *BMC genomics*, *13*(1), 1-11.

Modepalli, V., Fridrich, A., Agron, M., & Moran, Y. (2018). The methyltransferase HEN1 is required in Nematostella vectensis for microRNA and piRNA stability as well as larval metamorphosis. *PLoS genetics*, *14*(8), e1007590.

Moran, Y., Agron, M., Praher, D., & Technau, U. (2017). The evolutionary origin of plant and animal microRNAs. *Nature ecology & evolution*, *1*(3), 1-8.

Moran, Y., Fredman, D., Praher, D., Li, X. Z., Wee, L. M., Rentzsch, F., Zamore, P. D., Technau, U., & Seitz, H. (2014). Cnidarian microRNAs frequently regulate targets by cleavage. *Genome research*, *24*(4), 651-663.

Moran, Y., Praher, D., Fredman, D., & Technau, U. (2013). The evolution of microRNA pathway protein components in Cnidaria. *Molecular biology and evolution*, *30*(12), 2541-2552.

Plotnikova, A., Kellner, M. J., Schon, M. A., Mosiolek, M., & Nodine, M. D. (2019). MicroRNA dynamics and functions during Arabidopsis embryogenesis. *The Plant Cell*, *31*(12), 2929-2946.

Redfern, A. D., Colley, S. M., Beveridge, D. J., Ikeda, N., Epis, M. R., Li, X., Foulds, C. E., Stuart, L. M., Barker, A., & Russell, V. J. (2013). RNA-induced silencing complex (RISC) Proteins PACT, TRBP, and Dicer are SRA binding nuclear receptor coregulators. *Proceedings of the National Academy of Sciences*, *110*(16), 6536-6541.

Saito, K., Ishizuka, A., Siomi, H., & Siomi, M. C. (2005). Processing of pre-microRNAs by the Dicer-1–Loquacious complex in Drosophila cells. *PLoS biology*, *3*(7).

Schauer, S. E., Jacobsen, S. E., Meinke, D. W., & Ray, A. (2002). DICER-LIKE1: blind men and elephants in Arabidopsis development. *Trends in plant science*, *7*(11), 487-491.

Schmittgen, T. D., Lee, E. J., Jiang, J., Sarkar, A., Yang, L., Elton, T. S., & Chen, C. (2008). Real-time PCR quantification of precursor and mature microRNA. *methods*, *44*(1), 31-38.

Shaner, N. C., Lin, M. Z., McKeown, M. R., Steinbach, P. A., Hazelwood, K. L., Davidson, M. W., & Tsien, R. Y. (2008). Improving the photostability of bright monomeric orange and red fluorescent proteins. *Nature methods*, *5*(6), 545.

Song, L., Han, M.-H., Lesicka, J., & Fedoroff, N. (2007). Arabidopsis primary microRNA processing proteins HYL1 and DCL1 define a nuclear body distinct from the Cajal body. *Proceedings of the National Academy of Sciences*, *104*(13), 5437-5442.

Stocks, M. B., Moxon, S., Mapleson, D., Woolfenden, H. C., Mohorianu, I., Folkes, L., Schwach, F., Dalmay, T., & Moulton, V. (2012). The UEA sRNA workbench: a suite of tools for analysing and visualizing next generation sequencing microRNA and small RNA datasets. *Bioinformatics*, *28*(15), 2059-2061.

Tarver, J. E., Donoghue, P. C., & Peterson, K. J. (2012). Do miRNAs have a deep evolutionary history? *Bioessays*, *34*(10), 857-866.

Valli, A. A., Santos, B. A., Hnatova, S., Bassett, A. R., Molnar, A., Chung, B. Y., & Baulcombe, D. C. (2016). Most microRNAs in the single-cell alga Chlamydomonas reinhardtii are produced by Dicer-like 3-mediated cleavage of introns and untranslated regions of coding RNAs. *Genome research*, *26*(4), 519-529.

Varkonyi-Gasic, E., Wu, R., Wood, M., Walton, E. F., & Hellens, R. P. (2007). Protocol: a highly sensitive RT-PCR method for detection and quantification of microRNAs. *Plant methods*, *3*(1), 12.

Voinnet, O. (2009). Origin, biogenesis, and activity of plant microRNAs. *Cell*, *136*(4), 669-687.

Yamasaki, T., Onishi, M., Kim, E.-J., Cerutti, H., & Ohama, T. (2016). RNA-binding protein DUS16 plays an essential role in primary miRNA processing in the unicellular alga Chlamydomonas reinhardtii. *Proceedings of the National Academy of Sciences*, *113*(38), 10720-10725.

Zhong, J., Peters, A. H., Lee, K., & Braun, R. E. (1999). A double-stranded RNA binding protein required for activation of repressed messages in mammalian germ cells. *Nature genetics*, *22*(2), 171-174.

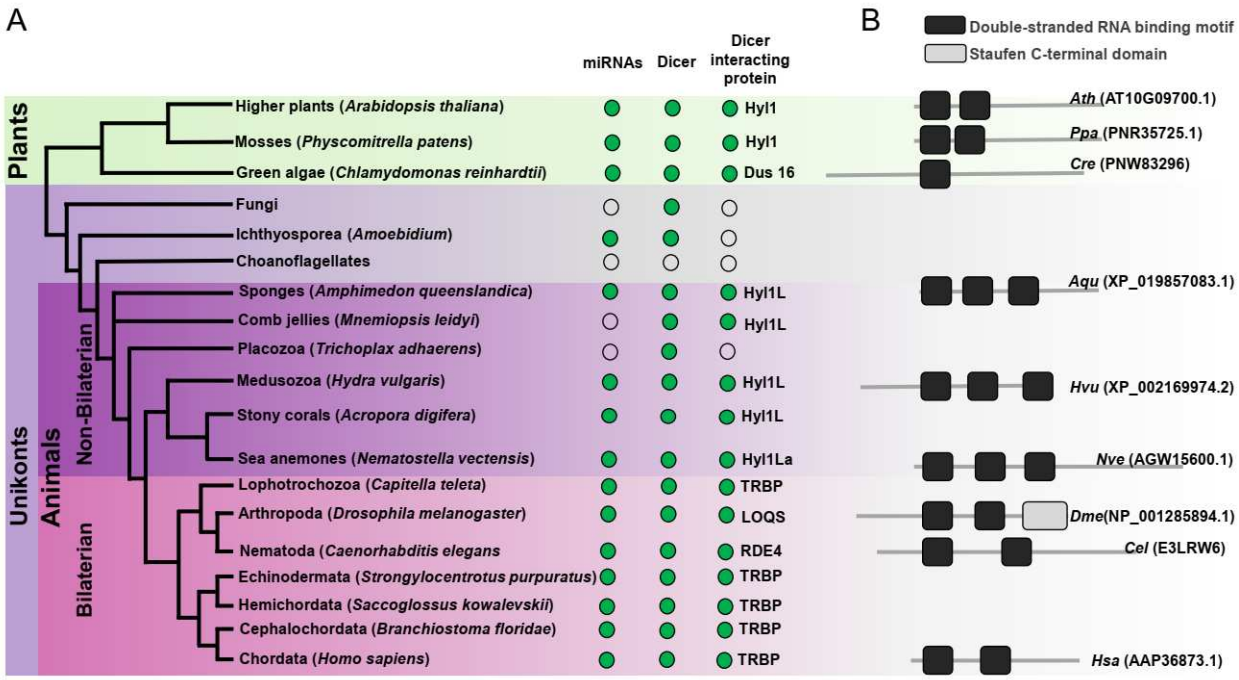

Figure 1. Schematic representation of a phylogenetic tree of Eukaryotes at the phylum level

(A) Phylogenetic tree representing the presence (green circles) and absence (open circles) of miRNAs, Dicer and Dicer interacting proteins in different plant and animal phyla. The names of often-studied organisms in different phyla are given in brackets. The names of Dicer interacting proteins are given near the green circles.

(B) Domain structure of different Dicer interacting proteins predicted by using the Pfam (https://pfam.xfam.org/). NCBI gene ID is shown in brackets.

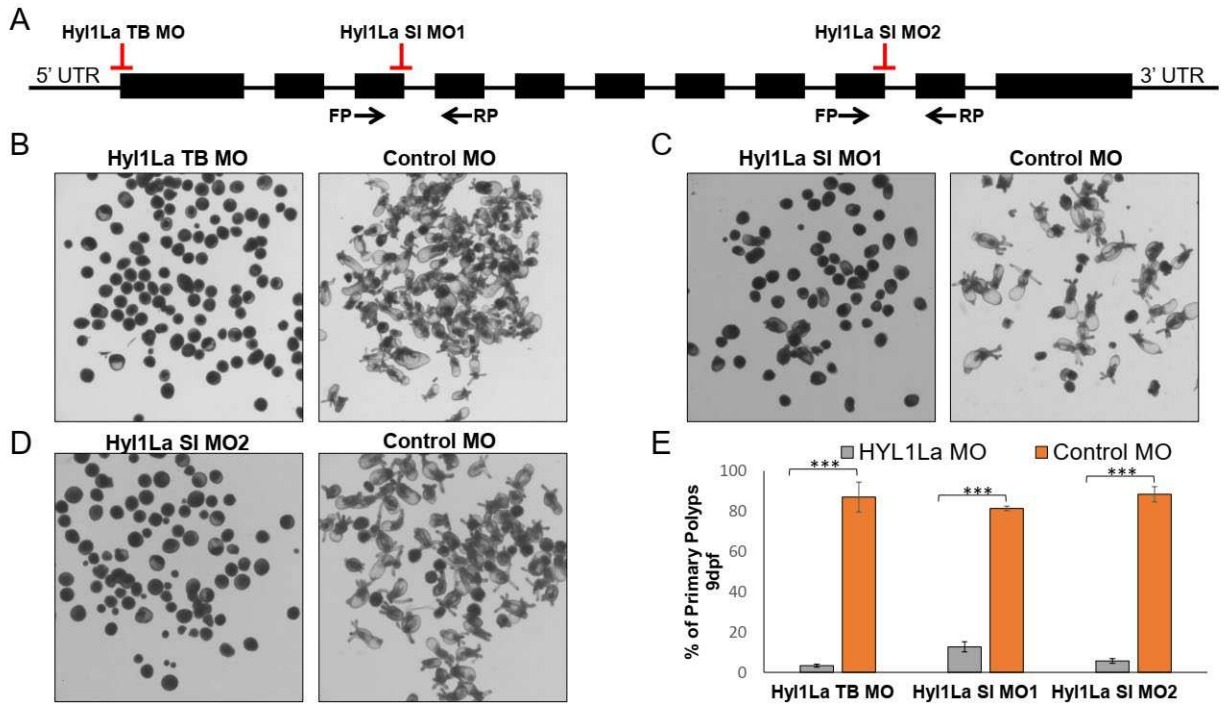

Figure 2. Developmental defects in different morphants of Hyl1La

(A) Schematic representation of the Hyl1La gene showing the intron-exon junction as defined by comparing the transcript (NCBI Accession KF192067.1) to the *Nematostella vectensis* genome. The positions targeted by different morpholinos used in the study are shown by red symbols. The black arrows represent the position of primers designed for the validation of splicing morpholino.

(B-D) Images of 9 dpf animals showing similar developmental defects in different morphants.

(E) Bar chart representing percentage of developed and undeveloped animals for each of the morphants. More than 80% of Hyl1La depleted animals did not develop into the primary polyp stage after 9 dpf. Data was taken in triplicates, in each n=200, ***P<0.001 (Student's t-test).

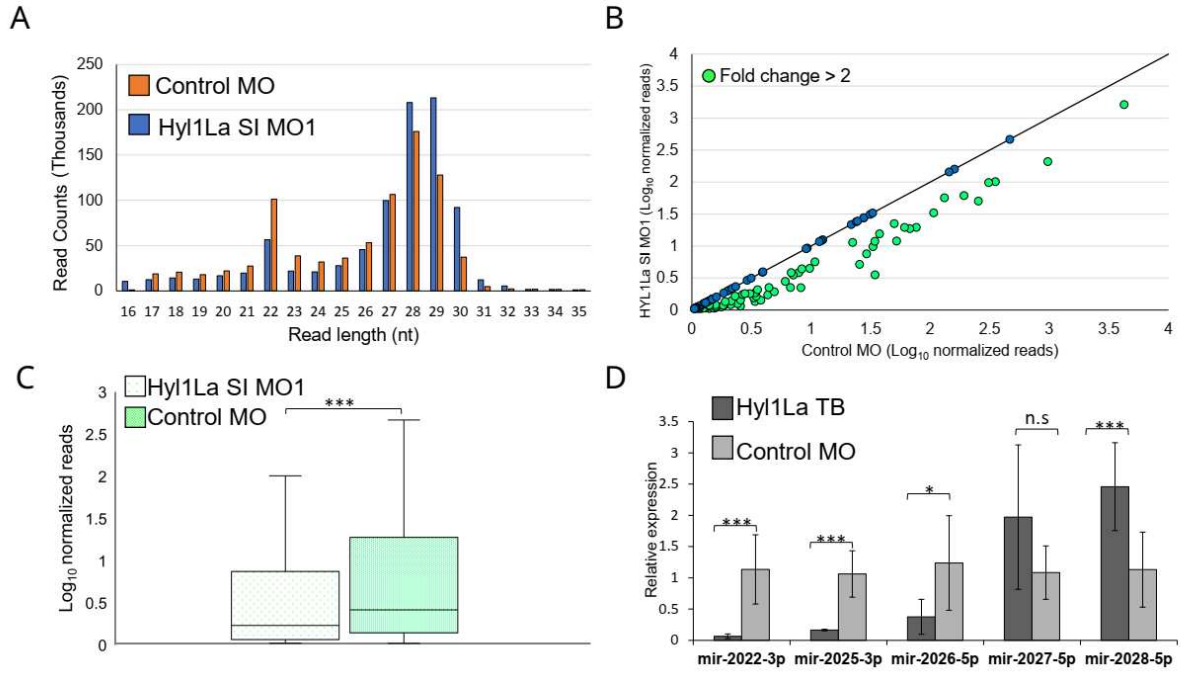

Figure 3. Hyl1La morphants show reduced expression of miRNAs

(A) Average read length distribution of small RNA reads after adapter removal.

(B) Scatter plot representing normalized read counts of miRNAs in control and treated animals. Each dot represents the average expression of an individual miRNA. The miRNAs showing a depletion greater than two-fold are indicated in green. The axes are scaled to Log_{10} of normalized read counts. The data represents the mean of three independent biological replicates.

(C) Box plot showing the average of abundance of miRNA read counts in Hyl1La SI MO1 and control MO. A significant reduction of miRNA read counts is noted in Hyl1La SI MO1, ($P < .0001$, Wilcoxon signed-rank test). The data represents the mean of three independent biological replicates ± SD.

(D) Bar plot showing the expression of miR-2022, miR-2025, miR-2026, miR-2027 and miR-2028 as quantified using stem loop PCR in translation blocking (TB) and control morpholino. The data represents the mean of three independent biological replicates ± SD. ***P<0.001, ** $P \leq 0.01$. * $P \leq 0.05$, (Student's t-test), n.s (not significant).

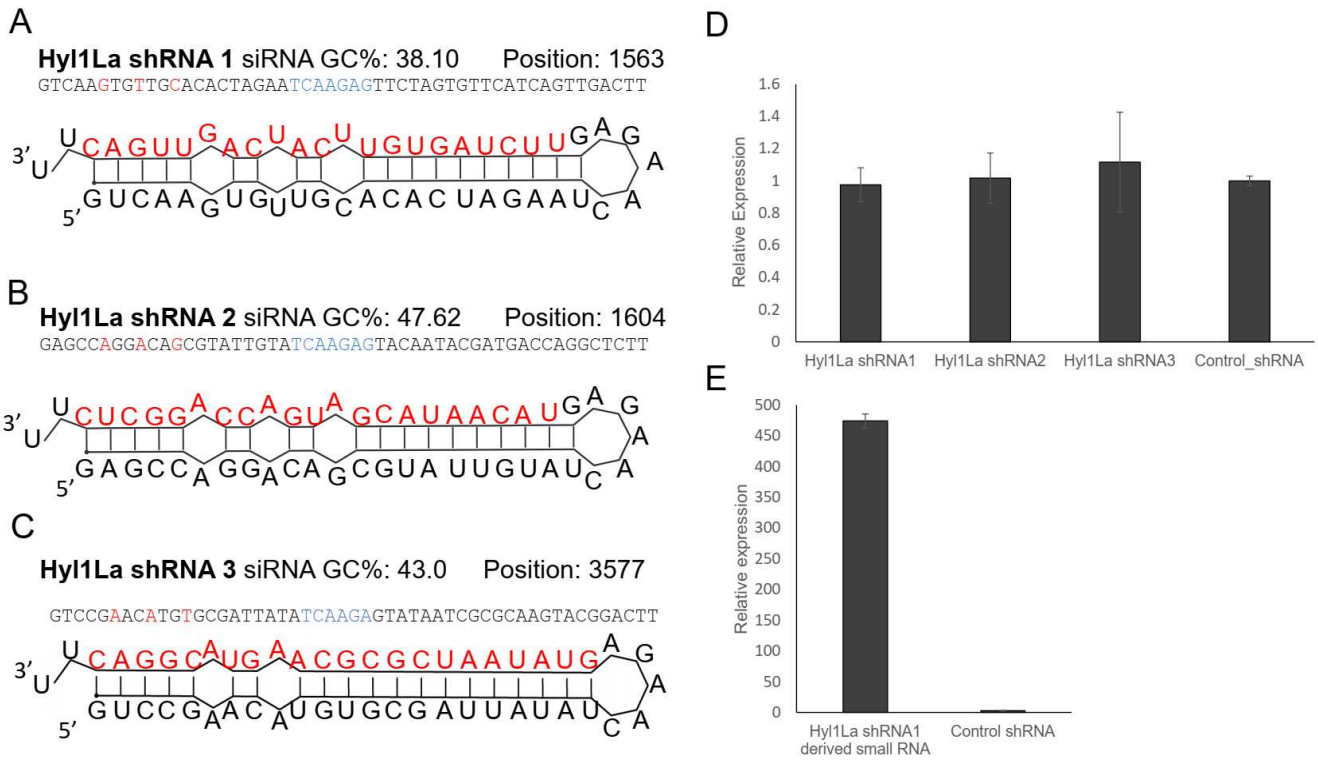

Figure 4. Structure of shRNA precursors and their effect on Hyl1La expression

(A-C) Structure of different shRNAs designed from different positions of Hyl1La gene along with GC content and their position are shown. In the shRNA sequence, the red colour shows the nucleotides edited for mismatch and blue colour represents loop region. The red coloured nucleotides on precursor's structure indicate the small RNA derived from the shRNAs.

(D) Real time quantification of Hyl1La from animals injected with different shRNAs relative to control. The data represents the mean of three independent biological replicates ± SD.

(E) Quantification of small RNAs produced from Hyl1La shRNA1. The quantification was performed by using stem loop qRT-PCR.

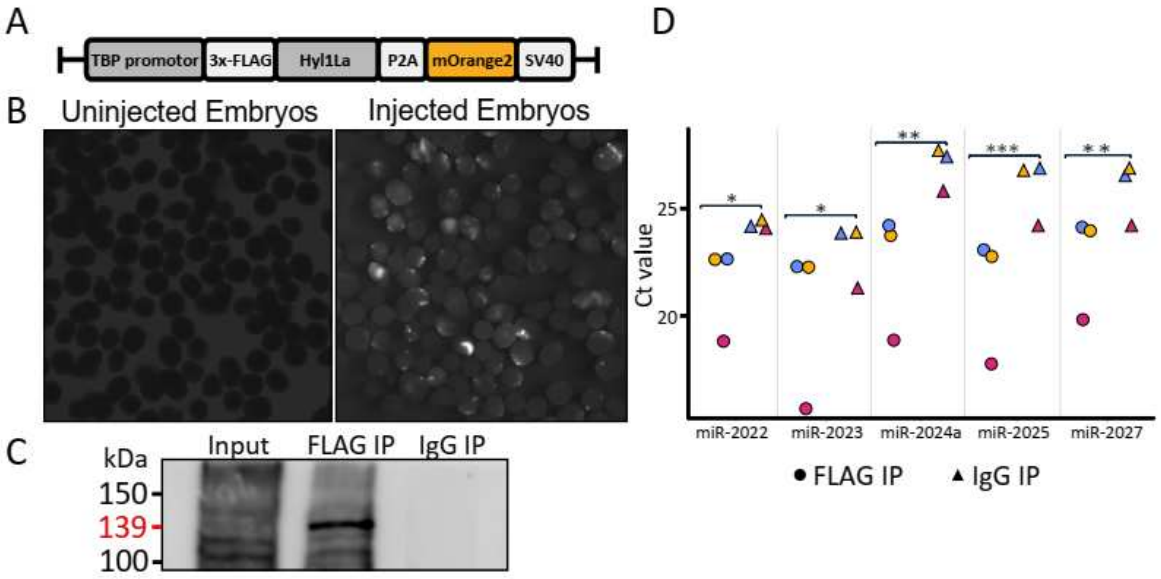

Figure 5. RNA Immunoprecipitation (RIP) and qRT-PCR

(A) Schematic representation of the FLAG-Hyl1La construct with a TBP promoter, a self-cleaving P2A sequence, a mOrange2 gene and the polyadenylation signal SV40.

(B) The plasmid-injected and uninjected embryos were visualized under a florescence microscope after two days. The injected embryos were showing the expression of mOrange2 (right side).

(C) Immunoprecipitation of 3×FLAG-Hyl1La with mouse anti-FLAG antibody or whole mouse IgG by using Protein G Magnetic Beads. The input and IP samples were subjected to Western blot with mouse anti-FLAG antibody. The red arrow (139 kDa) indicates the 3×FLAG-Hyl1La.

(D) pre-miRNA expression of five different miRNAs were measured using the qRT-PCR. The Y-axis represents the Ct-value of three independent biological replicates (each pair shown in a different color). ***P<0.001, **P ≤ 0.01. *P ≤ 0.05, (Student's t-test).

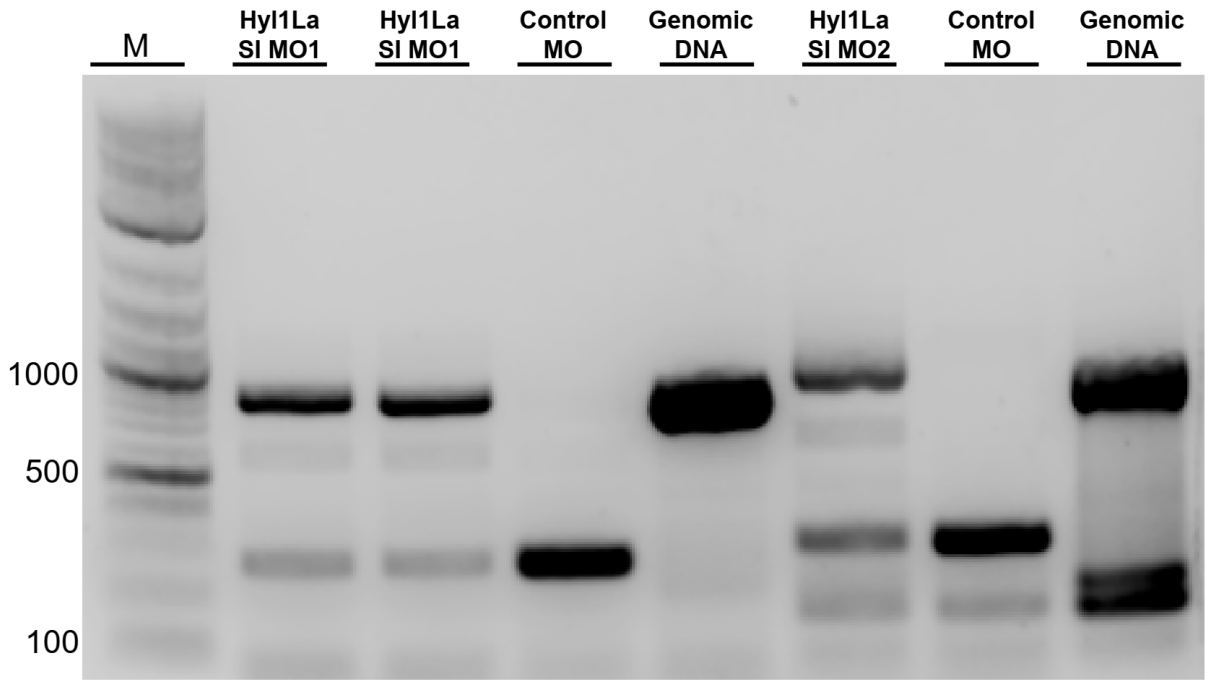

Figure S1. Gel image showing aberrant splicing of Hyl1La.

cDNAs were amplified by using two different primer sets for different morpholinos (Hy1La SI MO1 and Hyl1La SI MO2). The control morpholino lane showed the band of spliced Hyl1La while the Hyl1La SI morpholino lane showed the band of size equivalent for intron retention. The genomic DNA was amplified by using the same primer pairs to check the size and primer efficiency.

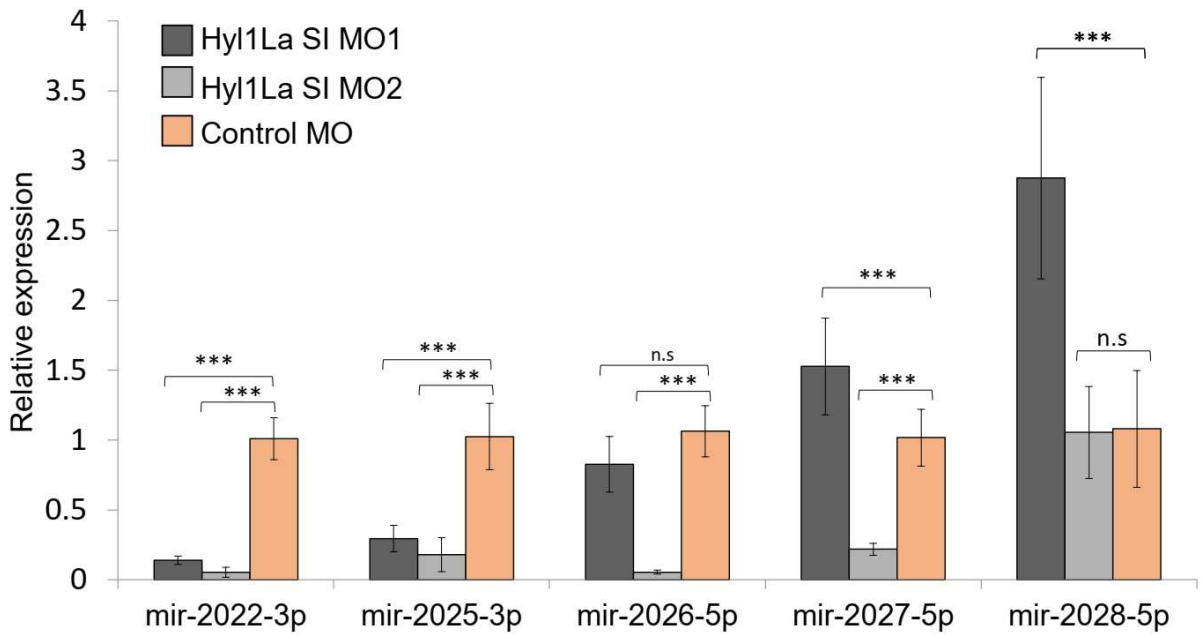

Figure S2. Effect of Hyl1La depletion on miRNA expression.

The expression of miR-2022, miR-2025, miR-2026, miR-2027 and miR-2028 were checked by using the stem loop PCR between the Hyl1La SI MO1 vs. Control MO and Hyl1La SI MO2 vs. Control MO. The data represents the mean of four independent biological replicates ± SD. ***P<0.001, ** P ≤ 0.01. * P ≤ 0.05, (Student's t-test), n.s (not significant).

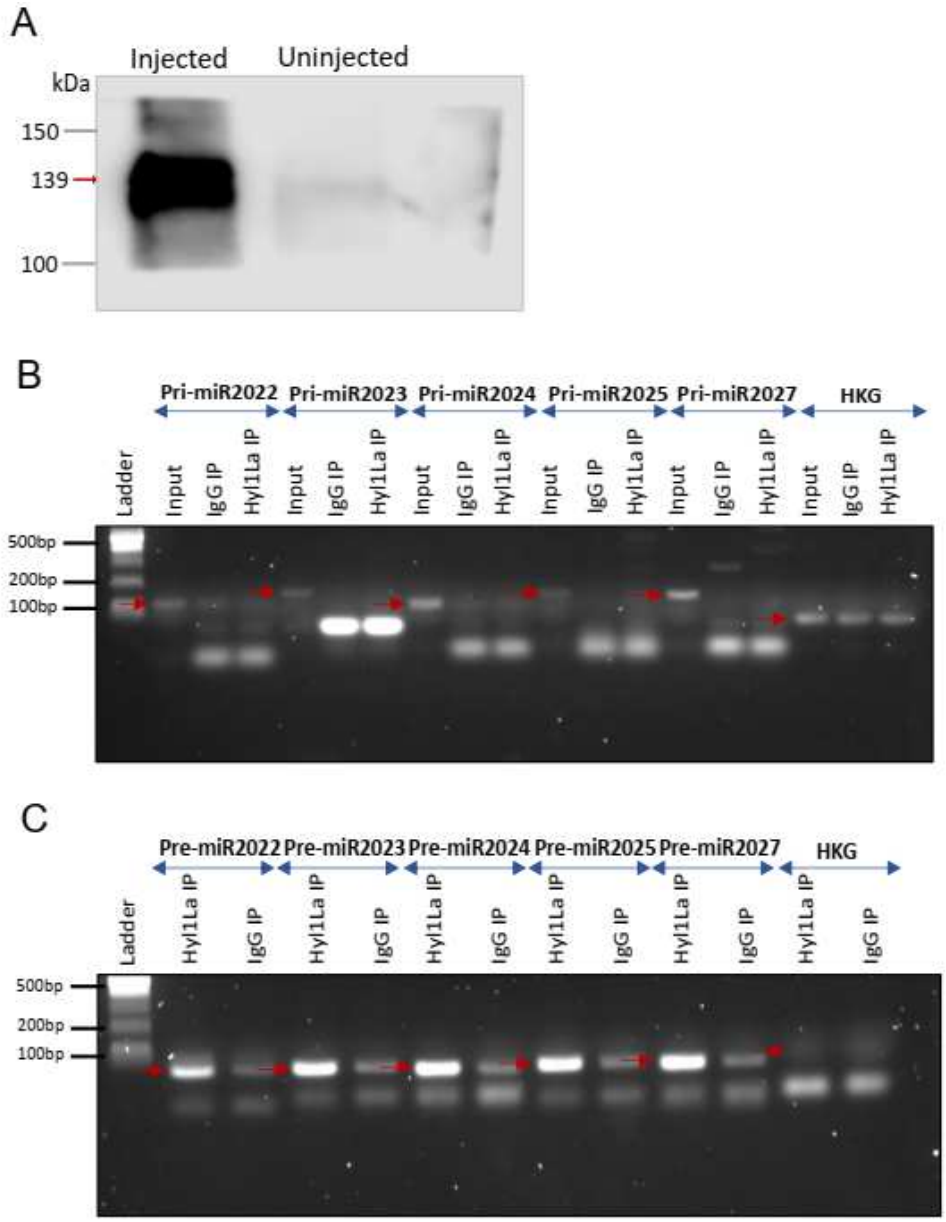

Figure S3. RNA Immunoprecipitation (RIP) and PCR

(A) Western blot of FLAG-tag-Hyl1La with mouse anti-FLAG antibody.

Gel image showing RT-PCR amplified (B) pri-miRNA (primary miRNA) and (C) pre-miRNA (precursor miRNA) transcripts. The pri- and pre-miRNA were amplified with their specific primers from RNA isolated from samples immunoprecipitated with mouse anti-FLAG antibody (Hyl1La IP)/whole mouse IgG (IgG IP). The red arrow indicates the expected product size. Ubiquitin was taken as control housekeeping gene (HKG).

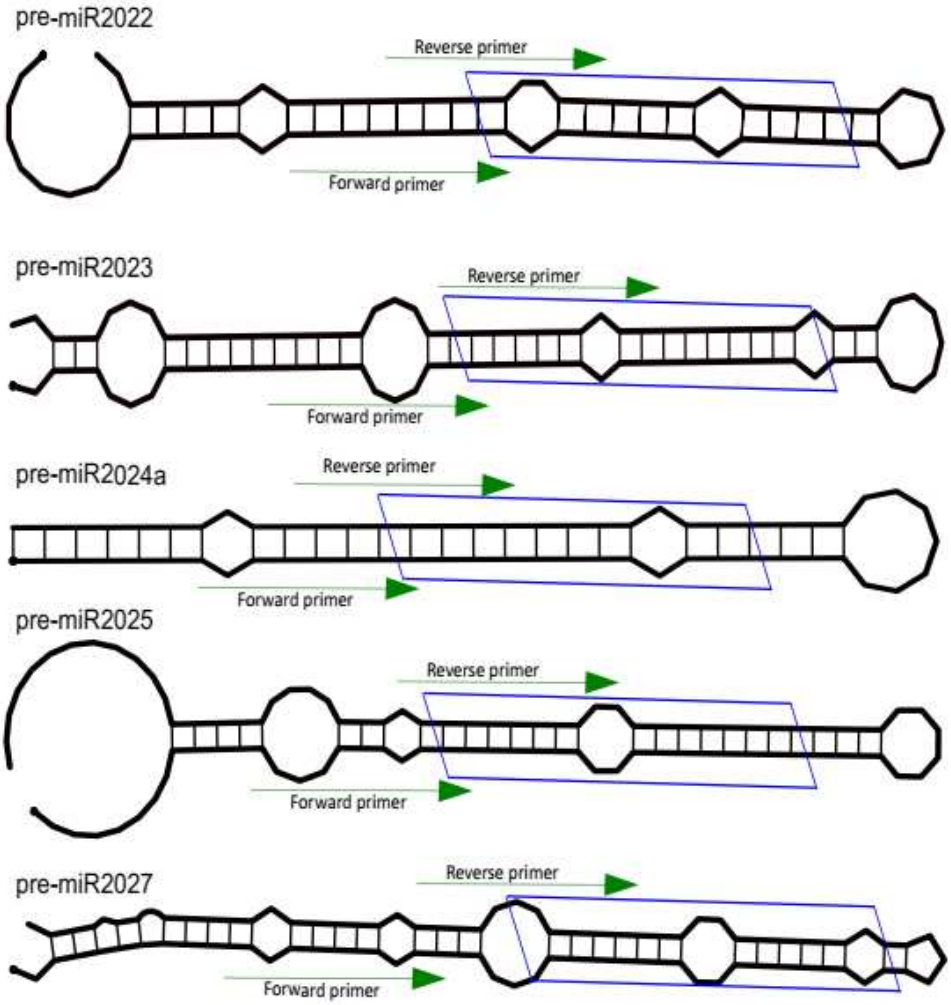

Figure S4. Position of primers on pre-miRNA

The secondary structure of miRNA precursors used in this study for identification of functional interaction with Hyl1La. The green arrow indicates the primer positions used for pri-miRNA quantification. The blue box represents position of miRNA/miRNA* duplex.

>nve-mir-2022

AGCGTGGGGATGCAGACAGATAATCTCGGGATGAGTTCGCCTGAATGATCAAGATGAGTTCGCCTGAA
AGTCGGGATGAGATCGCCTGAGAGTCGGGATAAGATCGCCTGAAAGTCGGGATAAATCAACTGTCAA
GTGGTTGTCATTTGCTAGTTGCTTTTGTCCCGCCTTTTCTGCGAATTGATCACGTGATGTGACGTCATCA
CTGCCCAATTACAAATGCTGCAATATATTGAGGTACGTAAACGTTAGATGTTGCGCATATACCTCATAC
G

>nve-mir-2023

GACTAGCTCAGTGGATCGACTAATTGGGGAATGGGCTATAGAAGACGACGATTACTATCAAAATAGCT
CAGTGGGCCAAGTACTGGAGACCAGACGAGAAGAGTTGCGTGACATACCTGTGTCTGCCACCTGTATT
TCTATCACGTCAGATGAAAGAAGTACAAGTGGTAGGGAAGGGTGTGTCGATTGACAATGGCGGCTTAT
CAAGACACGACCAATGTTGTAAGGGAGGAGGTAGATATACAAGAATGCAGCAGAAATAGTTTACAAG
CTTCGAGGTAAGGGAGGGAGTA

>nve-mir-2024a

CAAGAGCGATCGAGCACACGTGAGTCAGAATATTGCTTATGTTCTATAAGTATTCCTGGTAATTTTGAG
GAGGCGATGTAACTCTACCAACAAGTGCTACTGCTTCAAAATATCGGTGTTGGGTAAAAGGTCACATT
TTACACAGTACCGATATTGTGAAGCACGTTTGCTTAGGAACTAGGATACAACGAGGAGGCAAATTA
AAGCTACCAACAAGCGCTGTAACTCCACACGAAGACAGGTAACGAGAGAAATCAAGCCCG

>nve-mir-2025

GTAAAAGCATGTATGTGTTTTAACGCTAGTGCAGTAGCAAAACTACAACCGGGAGTGGAGACCCAAA
AGGCGTTCATGTCGACACAGCAAGAATATGATCAACAATTAGGCCACATACAAAGCTTTCGATGGCTA
GAAAATCCTTAGTGATTTTTTAGCCCGCGGAAGTTGTGTTGCCTGGCCAATATTACCATTAGGGTGAAG
GCAATGATCAAGACGAGGTTGTACTGGAAGACGCGAAGGCTGTTTATTTATATTACAGTATAAGGGTA
AGAAACATCGGTTACTTTGAAGG

>nve-mir-2027

CCTTGGAATCTCTCAGCTTCAAGAGCAGCAGCAAGCCCCTAGTAATTGATGTATTCAGTTTGTTTTCAA
ACAAGATAGAGCTGCACACCTCAGATCTTTCAATCCGAGAGCCTTAAGGCTT**GCTTGTTGGTAATTTT
GCATCT**GTTGCACATGCGATTTTACCAAAATGCAATTCTTATGGTTCAGTGATCAGGAACCCAATAAC
TGCAGCACAGTTGTCTGATATCGGTGCATGAAACTGATAGTCACTACAGTTTTTAAATTCATCTAATAT
AATAACTTCCAAGGGCTTATTT

Figure S5 Position of pre- and pri-miRNA primers on probable sequence of pri-miRNA

The probable sequence of pri-miRNA taken from the *Nematostella* genome browser (https://simrbase.stowers.org/). The underlined sequences represent the pre-miRNA. The sequences with purple and green colour represents primer position for pri- and pre-miRNA, respectively.